Optica Applicata, Vol. IX, No. 2, 1979

Diffraction images of truncated incoherent periodic objects in presence of primary coma

A. K. GUPTA, K. SINGH

Department of Physics, Indian Institute of Technology,
New Delphi-110029, India.

This paper deals with the investigations of the diffraction images of sine and square wave truncated incoherent periodic targets formed by the optical system suffering from primary coma. Graphical results along two different azimuths (i.e. $\psi = \pi/4$ and $\pi/2$) are presented to show the asymmetry and distortion in the images for varying amounts of aberration and numbers of cycles in the target. Table 1 is presented to give the modulation values for various numbers of cycles in the object and for various values of the aberration coefficient. Table 2 gives a comparative study of the contrast in the images of sine, square and triangular wave objects.

Introduction

Investigations on the images of periodic objects with finite number of cycles [1–9] are useful in connection with the accuracy of optical transfer function (OTF) measurements, detection of details in aerial photography and optical design. The targets having a finite number of cycles, such as two-bar or three-bar pattern are extensively used as resolution test targets in aerial photography [3, 4, 10, 11] and visual optical systems [12–14].

Motion degraded imagery of such objects for a variety of conditions has been studied by the group of authors [6–9]. In all the investigations, the optical systems may have some residual aberrations, off-axis aberrations in particulary. Recently CHANDRA et al. [15] have investigated the images of these targets in the presence of astigmatism.

Coma is also one of the most important off-axis aberrations and it is first to appear [16] where the field extends beyond the on-axis case. The asymmetric nature of this aberration is, in general, a very undesirable characteristic. Considerable amount of work on the evaluation of the images of the objects of the shape of infinite periodic, point, line, edge, disk and annulus in the presence of primary coma has already been done by several authors [17–24] and relevant references can be found in our recent papers [23, 24]. The effects of coma on visual optical systems has also been treated in [14].

The present paper is devoted to a study of the diffraction image of truncated sine and square wave targets in the presence of primary coma. A comparative study of the contrast in the images of sine, square and triangular wave profiles has also been given. The analysis is also being extended to partially coherent case and the results will be reported later.

Theoretical formulation

BARAKAT and LERMAN [1] have shown how to calculate the distribution of irradiance in the images of incoherent truncated objects. The spatial frequency spectrum $0(\omega)$ of the object is related to the intensity distribution $0(V)$ in the object by a Fourier transform relationship. For an object with N bars and period $4L$, $0(\omega)$ is given [1, 2] by

$$0(\omega)_{sq} = (2\pi\omega)^{-1} \frac{\sin(2N\omega L)}{\cos(\omega L)}, \tag{1}$$

$$0(\omega)\text{sine} = \pi(2\omega)^{-1}(\pi^2 - 4\omega^2 L^2)^{-1} \sin(2N\omega L), \tag{2}$$

$$0(\omega)_{tri} = (\pi\omega^2 L)^{-1} \tan(\omega L) \sin(2N\omega L). \tag{3}$$

The frequency spectra of image and object are related by

$$I(\omega, \psi) = T(\omega, \psi)\ 0(\omega). \tag{4}$$

Here $T(\omega, \psi)$ is the optical transfer function of the system under consideration, ψ being the angle formed by target lines with the meridian plane, i.e. azimuthal angle of target line structure, ω is the spatial frequency and L is the half width of the bright or dark portion in normalised units. $T(\omega, \psi)$ is generally a complex valued function [18]. Thus,

$$T(\omega, \psi) = T_r(\omega, \psi) + i\ T_i(\omega, \psi), \tag{5}$$

where T_r and T_i are the even and odd functions of ω, respectively. The final expression for irradiance distribution in the images of square wave target is given by

$$I(v, \psi) = (\pi)^{-1} \int_0^2 [T_r(\omega, \psi)\cos(V\omega) + T_i(\omega, \psi)\sin(V\omega)]0(\omega)_{sq}\, d\omega. \tag{6}$$

Here V is given in reduced units and related to the linear distance in the image plane by the equation $V = \pi x/\lambda F$, where F is f-number of the optical system, and λ is the wavelength of incident light. Similar expressions can be written for sine and triangular wave objects by inserting the appropriate expressions for $0(\omega)$.

The optical transfer function $T(\omega, \psi)$ for a circular aperture system in the presence of primary coma has been calculated by GOODBODY [17], and BARAKAT and HOUSTON [18]. We have calculated the transfer function in the presence of coma following the approach of BARAKAT and HOUSTON [18]. The final expressions for the transfer function are given by

$$T_r(\omega, \psi) = [T(0, 0)]^{-1} \int_{-a}^{a} \int_{-b}^{b} \cos\left[\frac{2\pi}{\lambda}\left\{W\left(\alpha + \frac{1}{2}\omega, \beta\right) - W\left(\alpha - \frac{1}{2}\omega, \beta\right)\right\}\right] d\alpha d\beta, \tag{7}$$

$$T_i(\omega, \psi) = [T(0,0)]^{-1} \int_{-a}^{a} \int_{-b}^{b} \sin\left[\frac{2\pi}{\lambda}\left\{W\left(\alpha+\frac{1}{2}\omega, \beta\right) - W\left(\alpha-\frac{1}{2}\omega, \beta\right)\right\}\right] d\alpha d\beta \tag{8}$$

where the limits of integration a, b are

$$a = \left(1-\frac{\omega^2}{4}\right)^{1/2}, \quad b = (1-\beta^2) - \frac{\omega}{2}, \quad 0 \leqslant \omega \leqslant 2, \tag{9}$$

and

$$W\left(\alpha+\frac{1}{2}\omega, \beta\right) - W\left(\alpha-\frac{1}{2}\omega, \beta\right) = 4\pi W_{31}\left[\frac{1}{8}\omega^3 \sin\psi + \frac{3}{2}\alpha^2\omega\sin\psi + \frac{1}{2}\omega\beta^2 \sin\psi - \alpha\beta\omega \cos\psi\right]. \tag{10}$$

Here W_{31} is the aberration coefficient and gives the number of wavelengths of aberration present.

The modulation M is the images is calculated by the formula

$$M = \frac{(\bar{I}_{max} - \bar{I}_{min})}{(\bar{I}_{max} + \bar{I}_{min})}, \tag{11}$$

where $\bar{I}_{max}$ has been taken as the mean of the two side maxima on both sides of the centre, and $\bar{I}_{min}$ denotes the closest minima on the either side.

The integrals occurring in equations (6), (7) and (8) are not easily amenable to analytical evaluation, hence for evaluating transfer function and intensity distribution numerical techniques have been used.

Discussion of the results

Figures 1–16 show the irradiance distribution in the images of periodic square and since wave truncated targets, with $N = 3$, 7, 11 and 15, for $L = 1.0$ and for varying values of aberration coefficient W_{31} along $\psi = \pi/4$ and $\pi/2$. For comparison purposes the intensity distribution in the ideal image has been represented by dotted curves in all the figures. It can be seen from the equation (6) that for $N = 1$, the problem is reduced to the case of single bar object. Therefore, we have also computed the results for a single bar which appeared to agree with those of BARAKAT and HOUSTON [20] in the presence of primary coma for various widths of the bar (i.e. for different values of L) along different azimuths. It is already known [1, 2] that in case of sine and square wave objects the general trend of the results is similar, hence the results will not be discussed separately.

It can be seen from the figures that there is shift in the position of peak intensity point which increases almost linearly with the increasing amount of aberration. The shift reaches its maximum along $\psi = \pi/2$ direction and becomes zero for $\psi = 0$, (which is not shown), being evident from the fact that in this case the imaginary part of the transfer function identically becomes zero. It is also observed that the intensity distribution is highly asymmetric with respect to the origin in the presence of large amount of aberration.

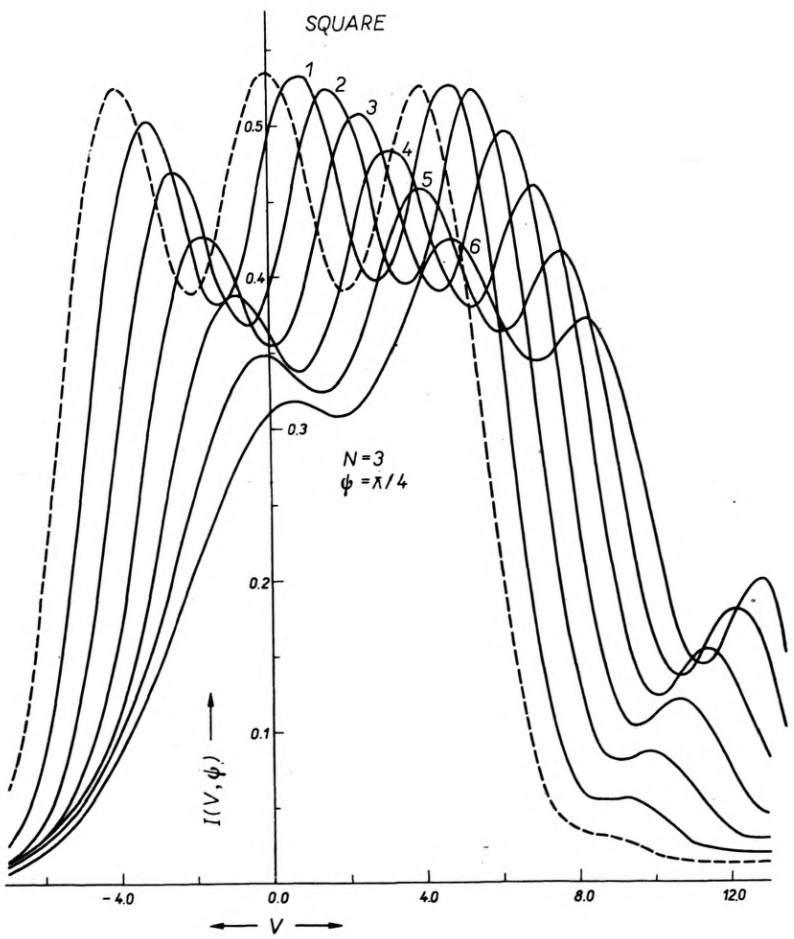

Fig. 1. Intensity distribution in the diffraction images of tribar targets ($N = 3$) along $\psi = \pi/4$ for different amounts of aberration

W_{31} = 0.25(*1*), 0.50(*2*), 0.75(*3*), 1.0(*4*), 1.25(*5*), 1.50(*6*)

For small number of target cycles the imagery of periodic bar pattern is appreciably affected by the presence of large amount of coma. For example, periodicity of the pattern is lost for $W_{31} = 2.0$ in figures 1 and 9. The tribar pattern behaves like an extended object (edge or single bar) for large magnitude of the aberration. This

is due to the fact that a high value of wave aberration removes a part of energy from bright portions of the image of an ideal bar target. One part of this energy is then distributed in the dark spaces between the bars and the remaining one spills over into the tails that appear at each end of the images. As W_{31} increases the amount of energy in the tail increases, while with the increase in N, it becomes smaller and smaller with respect to the total energy in the entire image. This increases the average irradian-

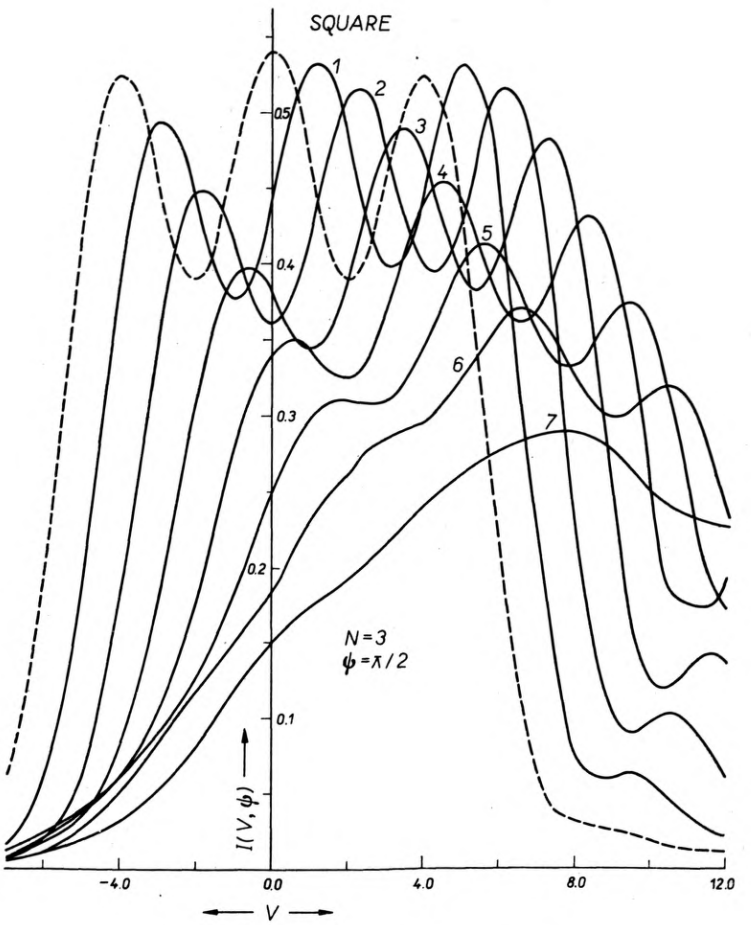

Fig. 2. Same as fig. 1 but for $\psi = \pi/2$
W_{31} = 0.25(*1*), 0.50(*2*), 0.75(*3*), 1.0(*4*), 1.25(*5*), 1.50(*6*), 2.0(*7*)

ce in the central region of the image which approaches asymptotically to 0.5 as N approaches ∞. The effect of coma on image quality of various objects can be better understood with the help of table 2 for modulation calculated with the help of equation (11).

Figures 1, 2, 9, and 10 clearly illustrate that in the case of an object with $N = 3$ the image is a poor approximation for the infinite periodic chain object. The two

maxima on either side of the central maxima do not rise to the level of the central maximum. Consequently, the usually defined contrast does not have a unique value, a point already mentioned by BARAKAT and LERMAN [1] and FOREMAN et al. [2]. As N increases e.g. $N = 7$, the side maxima rise to approximately the same level as the central maximum, hence they represent a better substitute to an infinitely

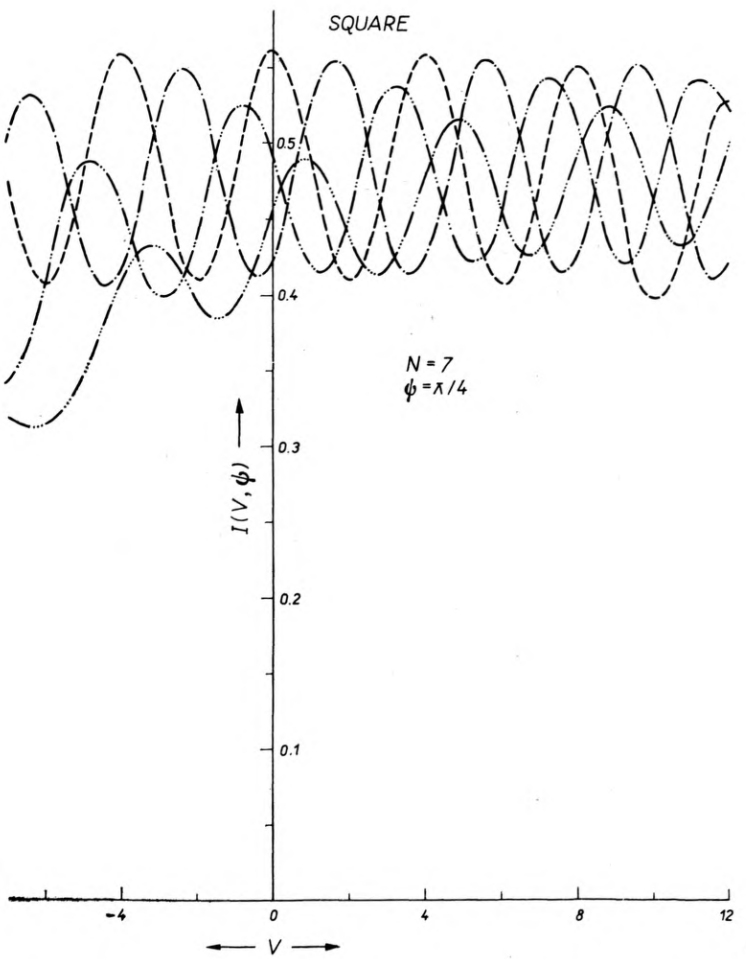

Fig. 3. Intensivity distribution in the diffraction images of truncated square target with $N = 7$ along $\psi = \pi/4$ for different amounts of aberrations

$W_{31} = 0.0(- - -)$, $0.5\ (-\cdot-)$, $1.0(- \cdot\cdot -)$, $1.5(- \cdots -)$

periodic object [1]. It is observed from the table 1 that for small amount of aberrations, e.g. $W_{31} = 0.5$ or 0.75 this still holds true but for higher values W_{31} (e.g. 1.5 or 2.0) the contrast values do not get stabilized and larger number of target cycles may be needed.

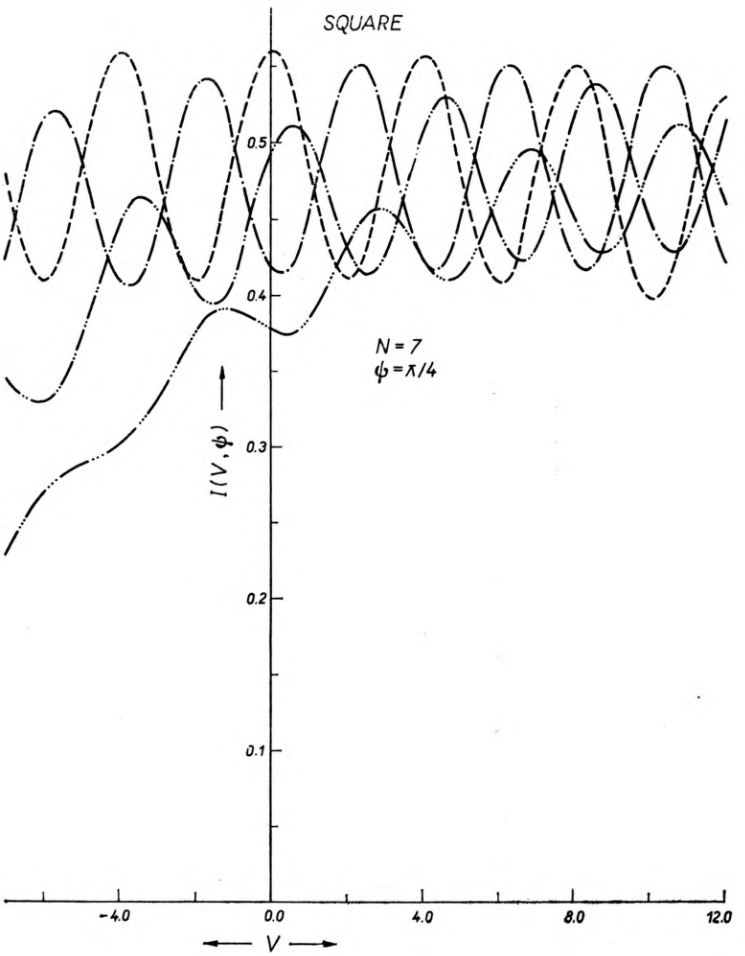

Fig. 4. Same as fig. 3 but for $\psi = \pi/2$
$W_{31} = 0.0$ (– – –), 0.5 (–·–), 1.0(–..–), 1.5(– ··· –)

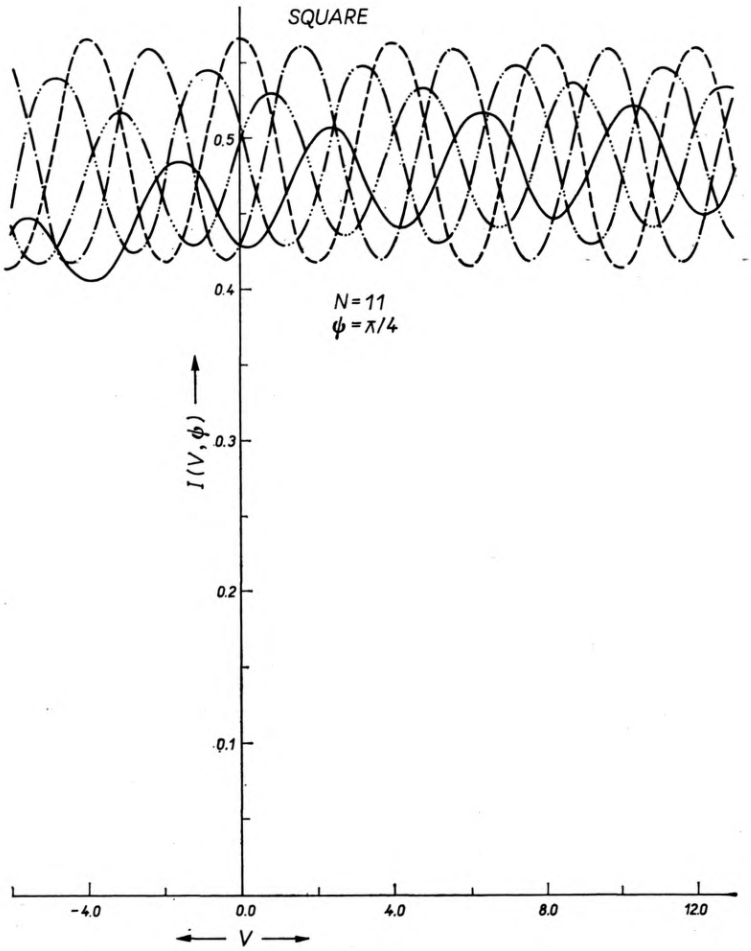

Fig. 5. Same as fig. 3 but with $N = 11$, and $\psi = \pi/4$
$W_{31} = 0.0$ (– – –), 0.5 (– · –), 1.0(– ·· –), 1.5 (– ··· –), 2.0(——)

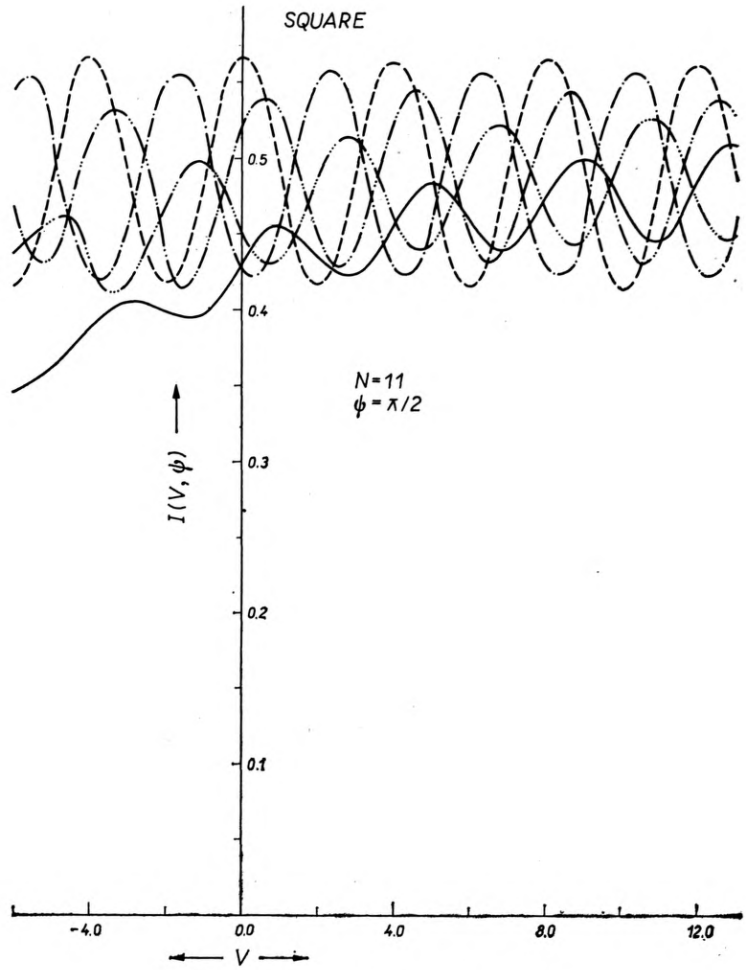

Fig. 6. Same as fig. 5 but for $\psi = \pi/2$

W_{31} = 0.0 (— — —), 0.5 (— · —), 1.0 (— ·· —), 1.5 (— ··· —), 2.0 (——)

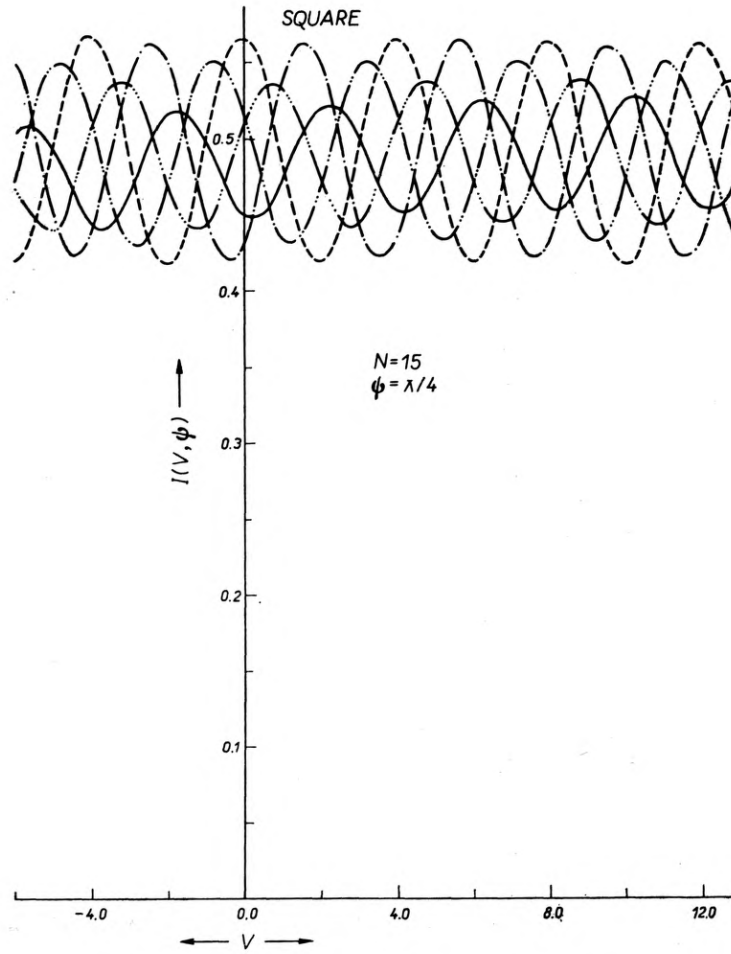

Fig. 7. Same as fig. 3 but with $N = 15$, and $\psi = \pi/4$
W_{31} = 0.0(— — —), 0.5 (— · —), 1.0 (— · · —), 1.5 (— · · · —) 2.0(——)

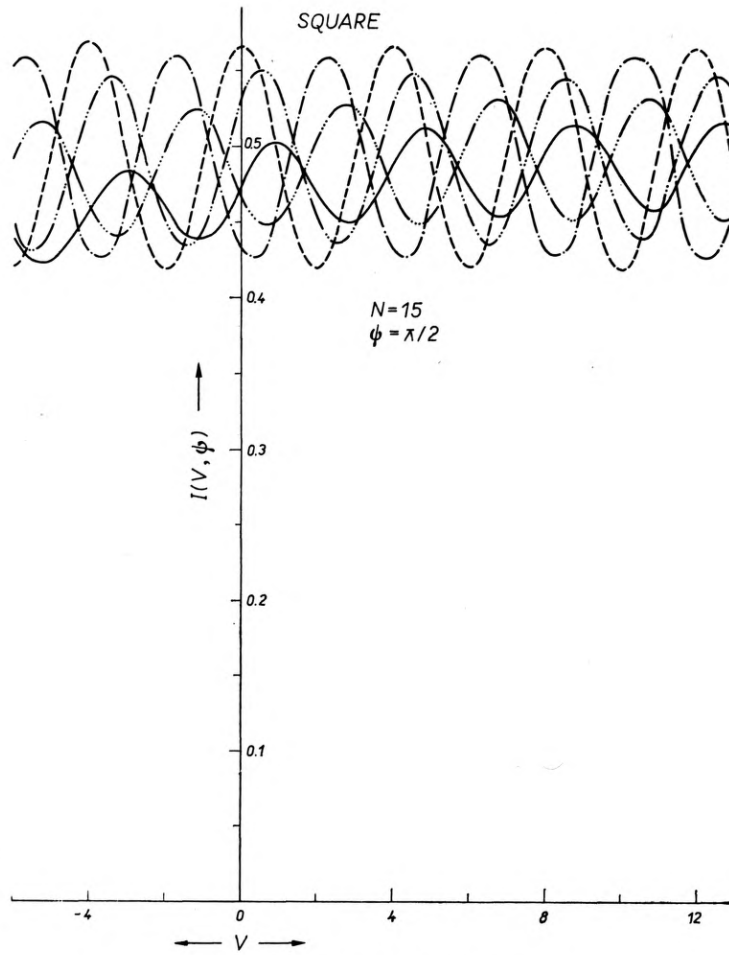

Fig. 8. Same as fig. 7 but for $\psi = \pi/2$

$W_{31} = 0.0(- - -)$, $0.5(- \cdot -)$, $1.0(- \cdot\cdot -)$, $1.5(- \cdots -)$ $2.0(——)$

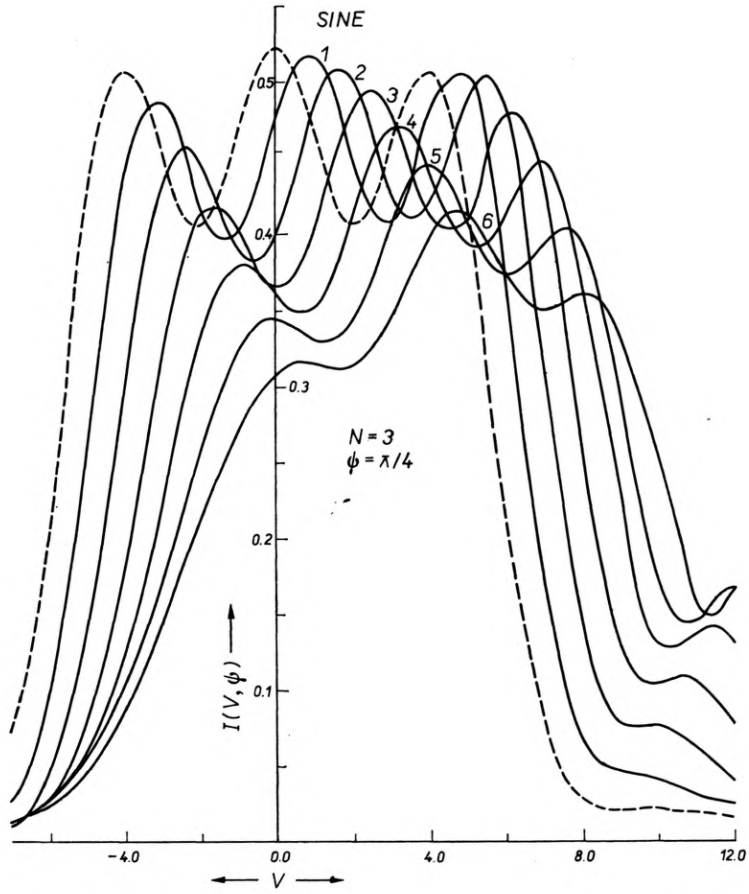

Fig. 9. Intensity distribution in the diffraction images of truncated sine wave target with $N = 3$ along $\psi = \pi/4$ for different amounts of aberrations

W_{31} = 0.25(*1*), 0.50(*2*), 0.75(*3*), 1.0(*4*), 1.25(*5*),1.50 (*6*)

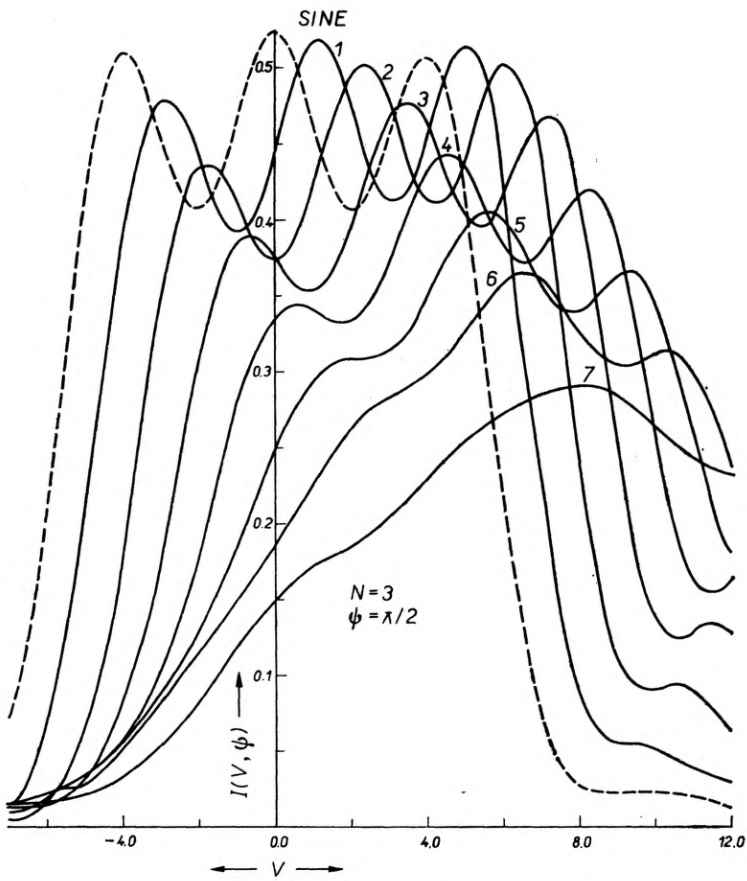

Fig. 10. Same as fig. 9 but for $\psi = \pi/2$

W_{31} = 0.25(*1*), 0.50(*2*), 0.75(*3*), 1.0(*4*), 1.25(*5*), 1.50(*6*), 2.0(*7*)

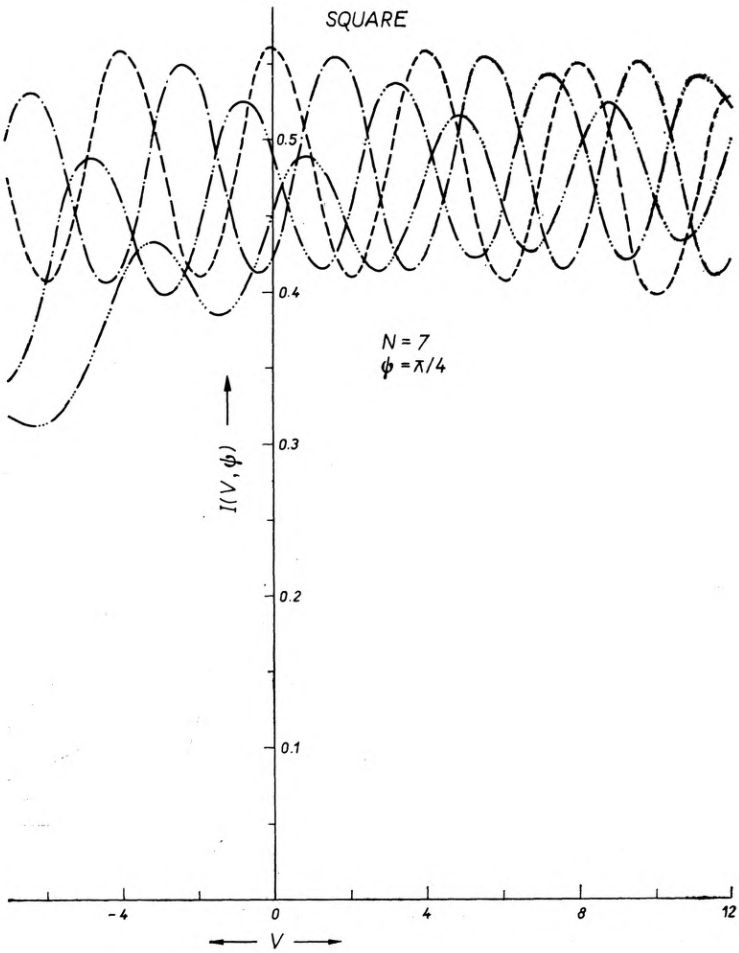

Fig. 11. Same as fig. 9 but with $N = 7.0$, and $\psi = \pi/4$
$W_{31} = 0.0$ (– – –), 0.5(– · –), 1.0(– ·· –), 1.5(– ··· –)

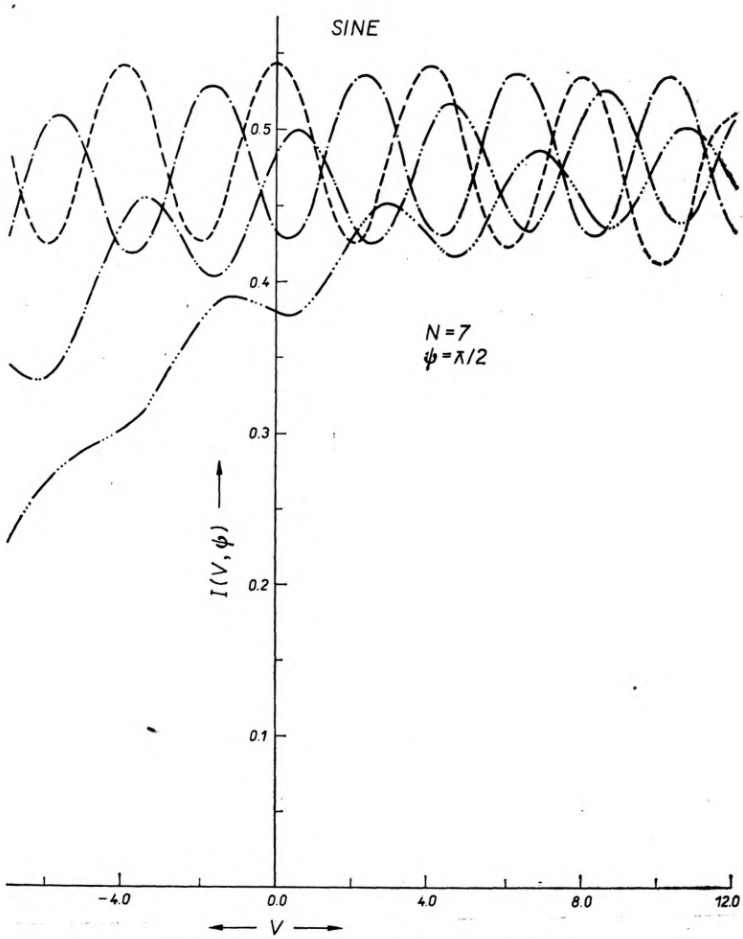

Fig. 12. Same as fig. 11 but for $\psi = \pi/2$

W_{31} = 0.0(— — —), 0.5(— · —), 1.0(— ·· —), 1.5(— ··· —)

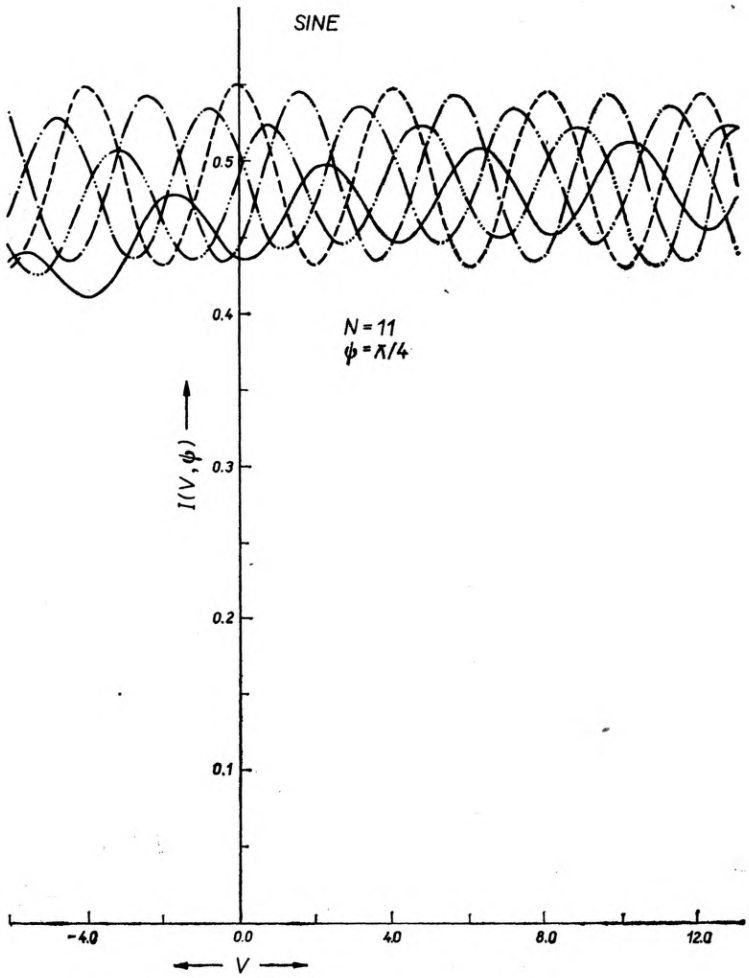

Fig. 13. Same as fig. 9 but with $N = 11.0$, and $\psi = \pi/4$
$W_{31} = 0.0(- - -)$, $0.5(- \cdot -)$, $1.0(- \cdots -)$, $1.5(- \cdots -)$, $2.0(——)$

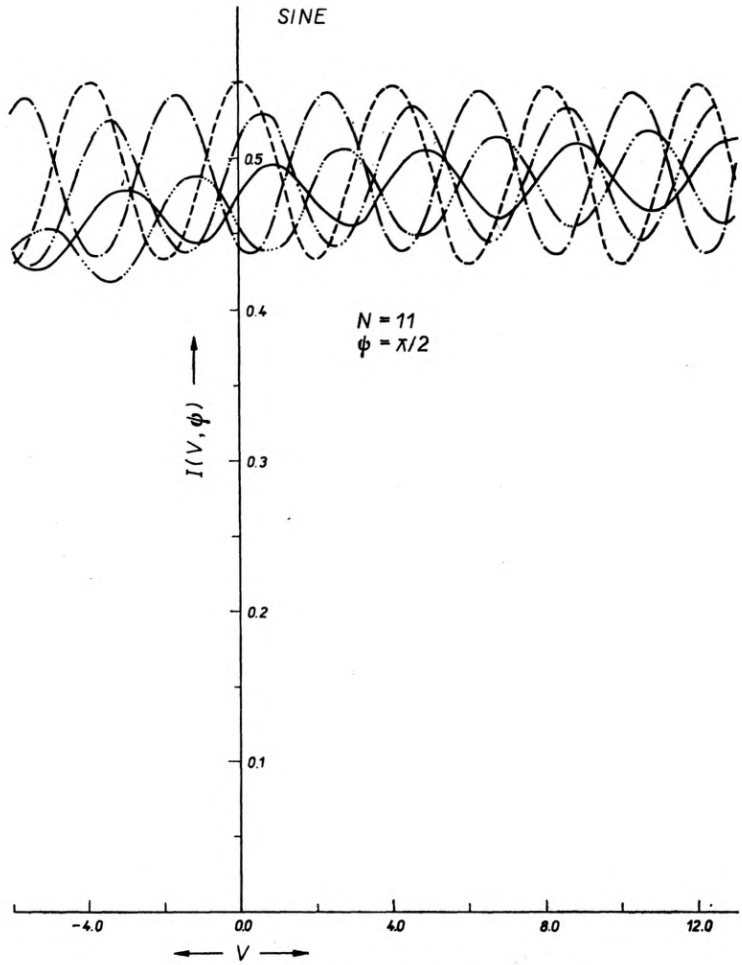

Fig. 14. Same as fig. 13 but for $\psi = \pi/2$

W_{31} = 0.0(– – –), 0.5(– · –), 1.0(– ·· –), 1.5(– ··· –), 2.0 (——)

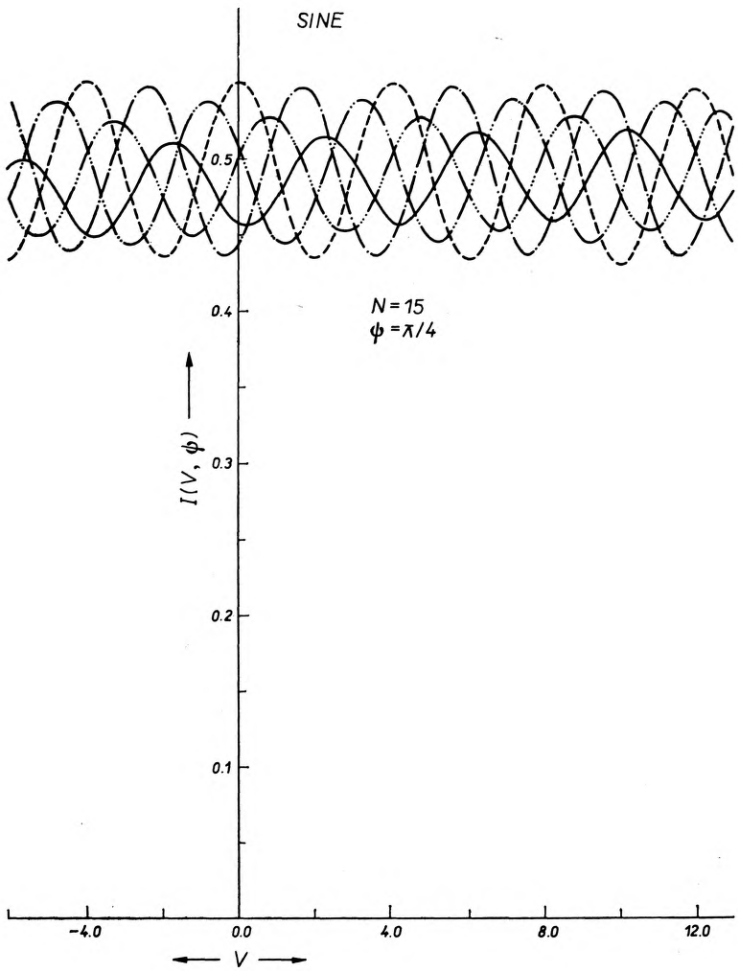

Fig. 15. Same as fig. 9 but with $N = 15$, $\psi = \pi/4$

W_{31} = 0.0(– – –), 0.5(– · –), 1.0(– · · –), 1.5(– · · · –), 2.0(——)

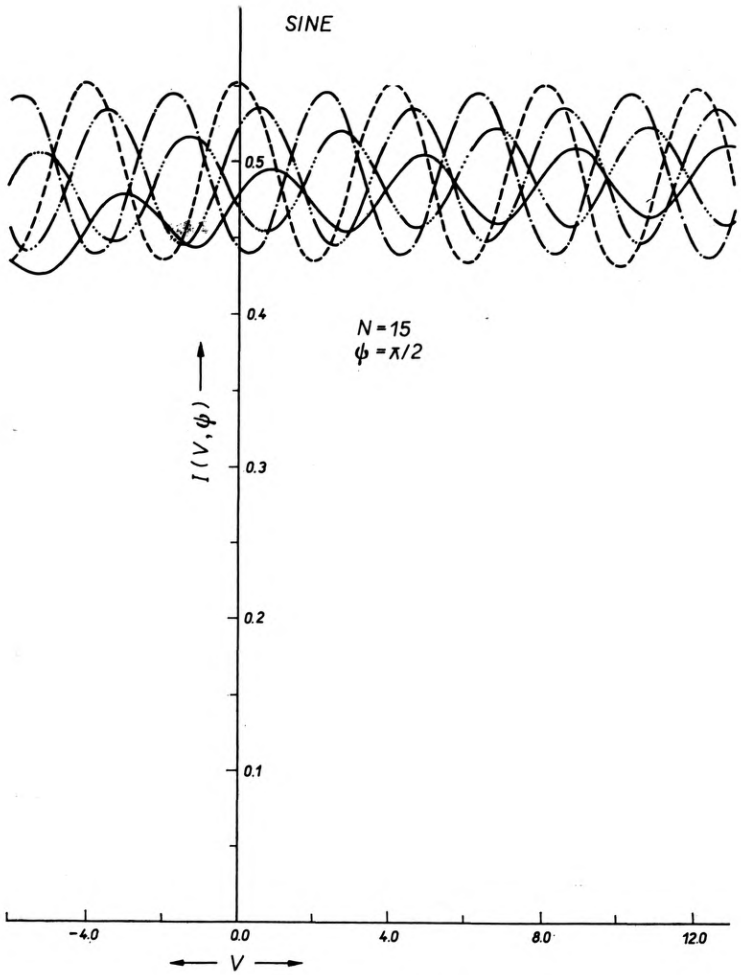

Fig. 16. Same as fig. 15 but for $\psi = \pi/2$

$W_{31} = 0.0(- - -), 0.5(- \cdot -), 1.0(- \cdot\cdot -), 1.5(- \cdot\cdot\cdot -), 2.0(——)$

Figures 17–19 show the contrast in the images of square, sine and triangular wave targets for $N = 15$ along $\psi = \pi/4$ and $\pi/2$ for $W_{31} = 0.5$, 1.0, and 1.5. The results for sine wave targets with $N = 15$ agree with the OTF results [18].

Table 1

Image contrast for sine and square wave targets in the presence of primary coma for $L = 1.0$

N	W_{31}	$\psi = \pi/4$		$\psi = \pi/2$	
		Modulation		Modulation	
		square	sine	square	sine
7	0.0	0.1514	0.1188	0.1514	0.1188
	0.25	0.1429	0.1121	0.1446	0.1135
	0.50	0.1416	0.1111	0.1326	0.1038
	0.75	0.1344	0.1053	0.1202	0.0989
	1.0	0.1167	0.0910	0.1036	0.0816
	1.25	0.1053	0.0867	0.0815	0.0640
	1.50	0.0911	0.0718	0.0596	0.0503
9	0.0	0.1502	0.1180	0.1502	0.1180
	0.25	0.1419	0.1114	0.1457	0.1132
	0.50	0.1409	0.1110	0.1281	0.1033
	0.75	0.1346	0.1009	0.1279	0.1003
	1.0	0.1183	0.0927	0.1108	0.0865
	1.25	0.1106	0.0884	0.0889	0.0698
	1.50	0.1015	0.0717	0.0715	0.0572
11	0.0	0.1496	0.1174	0.1496	0.1174
	0.25	0.1407	0.1104	0.1430	0.1123
	0.50	0.1403	0.1101	0.1314	0.1027
	0.75	0.1332	0.1045	0.1267	0.0994
	1.0	0.1176	0.0923	0.1140	0.0899
	1.25	0.1121	0.0879	0.0944	0.0739
	1.50	0.0914	0.0730	0.0759	0.0597
15	0.0	0.1496	0.1170	0.1490	0.1170
	0.25	0.1409	0.1107	0.1429	0.1123
	0.50	0.1400	0.1100	0.1309	0.1028
	0.75	0.1329	0.1045	0.1260	0.0991
	1.0	0.1168	0.0918	0.1125	0.0883
	1.25	0.1110	0.0873	0.0759	0.0747
	1.50	0.0913	0.0712	0.0779	0.0609

Table 2 gives the contrast for three types of targets with 15 cycles, and different values of the target frequency ($\omega_t = 2\pi/4L$). It is clear from the table 2, that the square wave targets are imaged with better contrast, as compared to the sinusoidal or triangular wave targets. However, the general trend of the results is the same in all the three cases. The contrast in the square wave and triangular wave targets

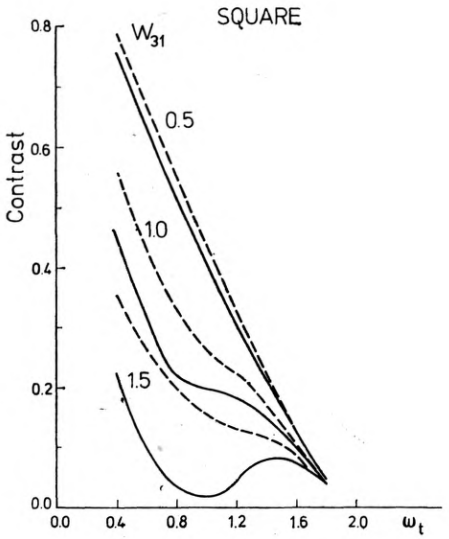

Fig. 17. Contrast of square wave targent with $N = 15$, $\psi = \pi/4$, $\pi/2$, and $W_{31} = 0.5$; 1.0; and 15.
– – – – $\pi/4$, —— $\pi/2$

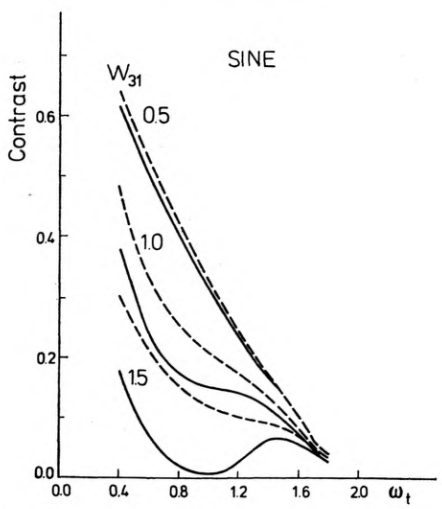

Fig. 18. Same as fig. 17 for sine wave target
– – – $\pi/4$, —— $\pi/2$

can also be calculated by evaluating the intensity distributions [25, 26] using the following expressions for infinitely periodic square and triangular wave targets.

$$I(V, \psi) = a - b + 2ab + \frac{4b}{\pi} \sum_{n=1}^{n'} T(n\omega, \psi) \frac{\sin(n\pi a)}{n} \cos(n\omega V) \qquad (12)$$

for square wave form, and,

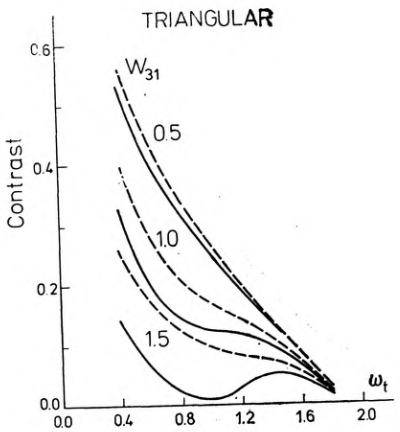

Fig. 19. Same as fig. 17 for triangular wave target
– – – $\pi/4$, ——— $\pi/2$

Table 2

Contrast in the images of truncated targets of square, sinusoidal and triangular wave profiles with $N = 15$

ω_t	W_{31}	$\psi = \pi/4$			$\psi = \pi/2$		
		Square	Sine	Triangular	Square	Sine	Triangular
0.5	0.4	0.7814	0.6410	0.5595	0.7539	0.6212	0.5317
	0.6	0.6691	0.5320	0.4321	0.6347	0.4994	0.4069
	0.8	0.5408	0.4251	0.3445	0.5139	0.4035	0.3217
	1.0	0.4256	0.3344	0.2708	0.4040	0.3174	0.2575
	1.2	0.3164	0.2385	0.1915	0.3058	0.2404	0.1947
	1.4	0.2185	0.1715	0.1389	0.2131	0.1675	01387
	1.6	0.1234	0.0970	0.0786	0.1228	0.0964	0.0812
	1.8	0.0466	0.0365	0.0297	0.0459	0.0360	0.0291
1.0	0.4	0.5615	0.4785	0.4000	0.4593	0.3836	0.3207
	0.6	0.4346	0.3311	0.2663	0.3177	0.2386	0.1907
	0.8	0.3255	0.2556	0.2071	0.2198	0.1727	0.1400
	1.0	0.2635	0.2073	0.1679	0.1954	0.1543	0.1252
	1.2	0.2245	0.1762	0.1428	0.1807	0.1420	0.1151
	1.4	0.1738	0.1363	0.1104	0.1525	0.1198	0.0971
	1.6	0.1081	0.0849	0.0687	0.0985	0.0733	0.0627
	1.8	0.0442	0.0346	0.02809	0.0424	0.0336	0.0270
1.5	0.4	0.3546	0.3063	0.2562	0.2170	0.1768	0.1389
	0.6	0.2661	0.2124	0.1736	0.0848	0.0659	0.0556
	0.8	0.2012	0.1580	0.1293	0.0348	0.0277	0.0229
	1.0	0.1553	0.1220	0.0989	0.0095	0.0075	0.0061
	1.2	0.1315	0.1032	0.0836	0.0439	0.0301	0.0285
	1.4	0.1179	0.0924	0.0749	0.0829	0.0651	0.0529
	1.6	0.0931	0.0732	0.0590	0.0788	0.0617	0.0396
	1.8	0.0411	0.0327	0.0257	0.03603	0.0285	0.0234

$$I(V, \psi) = a - b + 2ab + \frac{4b}{\pi} \sum_{n=1}^{n'} T(n\omega, \psi) \frac{\sin^2(n\pi a)}{n^2} \cos(n\omega V) \tag{13}$$

for triangular wave target.

Here $n = 1, 2, 3, \ldots, n'$; ab and $(1-a)\,b$ are the widths of the bright and dark bars; ω is the angular frequency and given by $\omega = 2\pi\nu$, where ν is the number of repetitive elements per unit distance so that the period is $b = 1/\nu$; a and b are the mean irradiance and modulation, respectively.

Additional remarks

JAISWAL and BHUSHAN [27] have shown that there is a non-linear relationship between the image contrast and object contrast (for the case when object contrast is less than one). In the present analysis the calculations have been carried out taking into account the unit contrast in the truncated targets. It would be useful to investigate the effect of varying the contrast in the truncated targets, as truncation error depends on the object contrast and the use of a test target of a lower contrast yields better results in the measurement of OTF.

Resolving power measurements in aerial photography or in visual optical systems are concerned with the images recorded on the films, or on the retina brain system [10, 14]. The limiting resolution in these cases is usually determined [3, 10, 14] by the point of intersection of the MTF curve of total optical system with the threshold modulation (TM) curves of the emulsion or the retina brain system. Tribar response is most widely used test target for the measurement of MTF-TM curves [10]. Tribar response in the present case can also be obtained by giving some more values to target frequencies ω_t. However sinusoidal periodic targets have also been used for this purpose. Hence our results may also be useful in setting the aberration tolerances or the resolution limits in the optical instruments used for the aerial photography and visual studies [10, 14].

Acknowledgement

We thank Prof. M. S. Sodha for his encouragement.

References

[1] BARAKAT R., LERMAN S., Appl. Opt. **6** (1967), 545.
[2] FOREMAN J. W., Jr., HUNT G. H., LAWSON E. K., Appl. Opt. **10** (1971), 105.
[3] BROCK G. C., *Image Evaluation for Aerial Photography*, Focal Press, London 1970.
[4] ARTISHEVSKII V. I., GRADOBOEV V. M., Sov. J. Opt. Tekh. **42** (1975), 672.
[5] Image Simulation Program (IMSIM), Optical Research Associate, USA (Developed by D. P. Paris of IBM).
[6] SINGH K., JAIN N. K., Nouv. Rev. Opt. **3** (1972), 309.

[7] SINGH K., RATTAN R., JAIN N. K., Appl. Opt. **12** (1973), 1846.
[8] SINGH R. N., SINGH K., Atti Fond. G. Ronchi **29** (1974), 727.
[9] GUPTA A. K., SINGH K., Current Science **42** (1975), 42.
[10] LAUROESCH T. S., FULMAR G. G., EDINGER J. R., KEENE G. T., KERWICK T. F., Appl. Opt. **9** (1970), 875.
[11] WILLIAMS R., Photo. Sci. Eng. **13** (1969), 252.
[12] SAVOY R. L., MCGANN J. J., J. Opt. Soc. Am. **65** (1975), 343.
[13] WESTHEIMER G., J. Opt. Soc. Am. **67** (1977), 207.
[14] GILES M. K., J. Opt. Soc. Am. **67** (1977), 634.
[15] CHANDRA A., SINGH K., SINGH R. N., Atti. Fond. G. Ronchi **30** (1975), 703.
[16] WELFORD W. T., *Aberrations of the Symmetrical Optical System*, Academic Press, London 1974.
[17] GOODBODY A. M., Proc. Phys. Soc. **75** (1960), 677.
[18] BARAKAT R., HOUSTON A., J. Opt. Soc. Am. **55** (1965), 1142.
[19] BARAKAT R., HOUSTON A., J. Opt. Soc. Am. **55** (1965), 1132.
[20] BARAKAT R., HOUSTON A., J. Opt. Soc. Am. **56** (1966), 1402.
[21] BARAKAT R., HOUSTON A., J. Opt. Soc. Am. **54** (1964), 1084.
[22] YZUEL M. J., BESCOS J., Opt. Acta **23** (1976), 329.
[23] GUPTA A. K., SINGH R. N., SINGH K., Can. J. Phys. **55** (1977), 1025.
[24] GUPTA A. K., SINGH K., Opt. Appl. **VII** (1977), 47.
[25] KOTTLER F., PERRIN F. H., J. Opt. Soc. Am. **56** (1966), 377.
[26] KATTI P. K., SINGH K., KAVATHEKAR A. K., Appl. Opt. **9** (1970), 129.
[27] JAISWAL A. K., BHUSHAN J., Appl. Opt. **13** (1974), 1839.

Received, August 4, 1978

Дифракционные изображения усеченных микрокогерентных дифракционных объектов при наличии первичной аберрации

Исследовались дифракционные изображения микрокогерентных испытаний в виде усеченных синусоидальных последовательностей или квадратичных волн, образованных оптическими системами, страдающими первичной комой. Показаны графические результаты вдоль двух разных факторов (т.е. $\psi = \pi/4$ и $\pi/2$) чтобы выявить асимметрию и дисторсию в изображении для разных значений аберрации, а также числа циклов в испытании. В таблице 1 представлены значения модуляции для разных чисел циклов в объекте и для разных значений коэффициента преломления. В таблице 2 дается сопоставление контраста в изображениях объектов в виде квадратных и треугольных синусоидальных волн.